

Prospecting MeerKAT Continuum Data for Enigmatic Radio Sources with Unsupervised Vector-Quantised Variational Autoencoders

Fernando L. Ventura,^{1,2} Kshitij Thorat,¹ Anna Bosman,³ Roger Deane,^{4,5,1} [★] Christopher Cleghorn⁶

¹Department of Physics, University of Pretoria, Private Bag X20, Pretoria 0028, South Africa

²Inter-University Institute for Data Intensive Astronomy

³Department of Computer Science, University of Pretoria, Private Bag X20, Pretoria 0028, South Africa

⁴Wits Centre for Astrophysics, School of Physics, University of the Witwatersrand, 1 Jan Smuts Avenue, Johannesburg, 2000, South Africa

⁵Inter-University Institute for Data Intensive Astronomy, Department of Astronomy, University of Cape Town, Cape Town, South Africa

⁶School of Computer Science and Applied Mathematics, University of the Witwatersrand, Jan Smuts Ave, Johannesburg, South Africa

21 January 2026

ABSTRACT

We present a novel application of Vector quantised variational autoencoders (VQ-VAEs) to deep 1.28 GHz radio continuum images taken from the MeerKAT Galaxy Cluster Legacy Survey (MGCLS). VQ-VAEs are deep learning models widely used in modern computer vision applications and pipelines. Designed for image generation, VQ-VAEs are trained to reconstruct the input dataset via a low-dimensional discrete embedding. VQ-VAEs effectively learn the distribution of training data, where samples that do not fit the distribution well yield the highest reconstruction errors. This property makes VQ-VAEs a good candidate for the task of anomaly detection. In this work, we examine the effectiveness of VQ-VAEs in identifying radio continuum sources with anomalous structures in the image-plane domain. We find VQ-VAEs to be useful as part of a solution for searching such large datasets. We observe that they are able to remove a majority of the typical sources in such data, even when trained in an unsupervised manner on unlabelled data. We also provide our testing set of a large sample of manually labelled radio sources, in particular radio galaxies, taken from the MGCLS at 1.28 GHz. Automated approaches to searching through high volumes of data are key in extracting the full scientific potential of the Square Kilometre Array and its pathfinders.

Key words: software: machine learning – radio continuum: galaxies – methods: data analysis

1 INTRODUCTION

Although machine learning (ML) is still relatively young in radio astronomy, it is expected to play a central role in addressing the field’s growing big-data challenges. A particularly relevant problem is the automated identification of exotic or anomalous sources in increasingly deep, wide, high-fidelity radio imaging surveys. Such anomalies are often of great scientific interest, as they may point to previously unrecognised astrophysical processes or rare transient phenomena. However, the definition of what constitutes an anomaly can be ambiguous and subjective, further complicated by the fact that physically unusual sources may not be visually distinct in imaging data.

Unsupervised and semi-supervised ML methods, such as autoencoders (AEs), offer a promising avenue for anomaly detection in astronomy due to their ability to learn compact representations of data without requiring extensive labelled datasets (Han et al. 2022; Alonso et al. 2024; Brand et al. 2025). AEs consist of two parts, an encoder model and a decoder model. The encoder compresses the input data into a low-dimensional latent space and the decoder subsequently reconstructs the input data. The reconstruction error

can serve as a proxy for novelty. In this approach, simple, common sources are easily reconstructed with low residual error.

In convolutional AEs, the encoder and decoder are convolutional neural networks (CNNs). CNNs are multi-layered neural networks designed to learn spatial correlations between neighbouring input signals. As an input image is passed through the model, the input for each layer is convolved by some kernel to produce the output which serves as the input for the next layer. The kernel weights are iteratively adjusted during training to minimise the reconstruction error.

Variational autoencoders (VAEs) and their discrete counterparts, vector-quantised VAEs (VQ-VAEs) (van den Oord et al. 2017), improve upon classical AEs by learning structured latent representations that are more amenable to clustering and generative tasks (Van Den Oord et al. 2017). VQ-VAEs, in particular, are capable of learning a discrete codebook of latent embeddings, making them well-suited to anomaly detection, where clear distinctions between common and rare patterns are desirable (Marimont & Tarroni 2021; Gangloff et al. 2022).

The application of ML techniques for anomaly detection in astronomy has gained significant attention, particularly with the advent of large-scale surveys that produce vast amounts of data (Lochner & Bassett 2021; Giger & Csillaghy 2024; Lochner & Rudnick 2025).

[★] E-mail: roger.deane@wits.ac.za

Traditional approaches, such as AEs and VAEs, have been employed to model the distribution of “normal” data, and identify deviations indicative of anomalies (Doorenbos et al. 2021; Andrianomena & Tang 2024; Brand et al. 2025). Doorenbos et al. (2021) compared AEs, including convolutional AEs, to four other ML approaches for use in anomaly detection to outlier detection on the Sloan Digital Sky Survey (SDSS). They found that when comparing a suite of algorithms, AEs selected the most distinct sample of outliers. Brand et al. (2025) performed further comparisons between convolutional AEs and traditional ML techniques for the purpose of anomaly detection in radio astronomical data, and concluded that AEs outperformed conventional ML when trained on independent principal components extracted from the data.

VQ-VAEs, schematically illustrated in Figure 1, offer several key advantages over standard AEs and VAEs for anomaly detection (Marimont & Tarroni 2021; Gangloff et al. 2022), particularly in domains like astronomy, where the structure and diversity of the data are high, and anomalous sources may only be subtly different. These advantages stem primarily from the nature of latent space representation of VQ-VAEs, which is discrete and quantised, as opposed to continuous and often entangled in standard AEs and VAEs (Van Den Oord et al. 2017). Continuous latent spaces can lead to overlapping representations of semantically distinct features, which reduces their sensitivity to anomalies, especially in high-dimensional data such as astronomical images, where the range of “normal” morphologies is broad. VQ-VAEs, on the other hand, learn a discrete latent codebook: each input is mapped to the nearest prototype in a learned codebook of embeddings. This induces a more clustered, interpretable, and robust representation, where normal patterns form tight groups, and deviations stand out more clearly (Van Den Oord et al. 2017). In VQ-VAEs, when an input is significantly different from the training distribution, it may be forced to employ seldom-used or novel codebook combinations, or yield a high reconstruction loss due to a poor match with the existing codebook. This behaviour is beneficial for anomaly detection: the model inherently signals when an input does not align well with learned normal patterns, either by elevated reconstruction error, low codebook usage frequency, or activation of rare latent codes (Marimont & Tarroni 2021; Gangloff et al. 2022).

In the medical imaging domain, VQ-VAEs have been successfully applied to detect anomalies in optical coherence tomography angiography (OCTA) images, demonstrating their potential to identify subtle pathological features (Jebrel et al. 2024). Similarly, Pinaya et al. (2022) combined VQ-VAEs with an ensemble of Transformer networks to detect anomalies in 3D brain imaging. These studies underscore the potential of VQ-VAEs to capture complex data distributions and detect anomalies in real-world domains.

In this paper, we explore the feasibility of using VQ-VAEs as an off-the-shelf architecture for anomaly detection in radio astronomical data. We use the MeerKAT Galaxy Cluster Legacy Survey (MGCLS, Knowles et al. 2022), from which we create a catalogue of labelled sources, as well as many unlabelled sources as identified by source-finding software. The labelled sources are manually labelled into typical and exotic sources. Although the definition of an exotic source is subjective, we attach the label to those sources which we believe are scientifically interesting due to their scarcity or how unusual they may be. For instance, we label X-shaped sources as exotic, while bent sources, common FRIs, and FRIIs are labelled typical. A physically anomalous source may well have a visually typical appearance. We investigate how well a convolutional VQ-VAE can find exotic sources in the data. We test two main configurations of a VQ-VAE, one of which is semi-supervised and trained only on the smaller set of labelled typical sources, while the other is

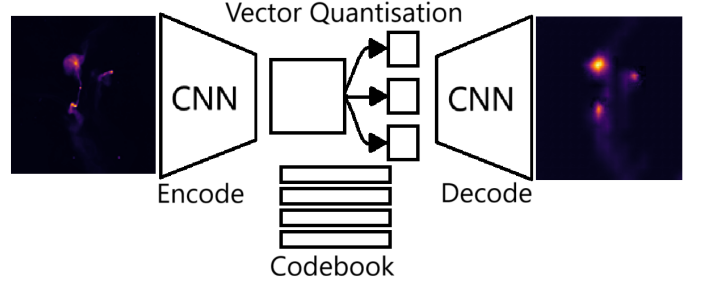


Figure 1. Basic structure of a VQ-VAE. The encoder reduces the input to the dimensions of the latent space. A code form is produced from a learned codebook of discrete vectors. The decoder attempts to reconstruct the original input from the code form.

trained in a fully unsupervised manner on the larger set of unlabelled data. The manually labelled sources are used to evaluate the relative effectiveness of either configuration.

2 DATA

To test the utility of VQ-VAE’s specifically for SKA precursor data, we chose the publicly available MeerKAT Galaxy Cluster Legacy Survey (MGCLS) Stokes-I images. MGCLS is formed of deep MeerKAT images of 115 galaxy clusters with high fidelity in the L-band (900–1670 MHz). Each cluster field was observed for about 6 to 10 hours in full polarisation mode. Each image has a central observing frequency of 1.28 GHz with typical sensitivity ranging from about 3 to 5 μ Jy/beam and imaging dynamic range of order 10^{4-5} . The images have a typical angular resolution of ~ 10 arcsec and high sensitivity to structures up to about 10 arcmin scales. The basic full-field spectral cubes span about 2 deg \times 2 deg while the enhanced products consist of the inner 1.2 deg by 1.2 deg field of view corrected for the primary beam. A wide field of view means there are hundreds to thousands of non-cluster sources per image. The compact source catalogue, presented in Knowles et al. (2022), contains approximately 626,000 sources, not counting the more challenging extended, diffuse sources whose environments are “contaminated” with these often unrelated compact / point sources. It should be noted that these images as such are fundamentally different from a perspective of spatial source density and complexity from typical samples which use samples from older surveys such as Faint Images of Radio SKy at Twenty Centimeter (FIRST) and NRAO-VLA Sky Survey (NVSS) (see Becker et al. 1995) and Condon et al. 1998 respectively), and therefore closer to the images which we may expect from the upcoming SKA.

The galaxy cluster images are processed to find extended sources using the source-finding software PyBDSF¹. PyBDSF searches for and models sources in the larger image using ellipses, which it groups into islands of emission which may represent an extended source. The thresholds for included emission and grouping are adjusted by trial and error until PyBDSF produces a catalogue containing most extended sources.

We take cutouts of the sources with the sizes and centre of the cutouts being estimated from the PyBDSF output, and may therefore

¹ <https://github.com/lofar-astron/PyBDSF>

be imperfect. We manually classify a subset of these sources, labelling them as “typical” or “exotic”. During manual inspection, we flag images that have cutouts that may need to be removed, as they require adjustment or are point sources. An excerpt from the full table we have used is shown in Table 1.

We do not further adjust these cutouts in our labelled sample in order to keep it consistent with the unlabelled data for training purposes, as well as to be representative of a real-world use case, where large quantities of data would need to be processed in an automated manner. However, adjusted cutouts are made for the released dataset.

Our final sample consists of 13821 unlabelled sources, 2049 labelled typical sources, and 58 labelled exotic sources. We provide the labelled dataset of 2107 sources on Zenodo² publicly as a community resource which will be updated with successive data releases adding more classification tags as well as more sources.

3 METHODOLOGY

3.1 Vector Quantised Variational Auto-Encoders

We use the VQ-VAE implementation created by Sayak Paul³ for Keras⁴ as described in [van den Oord et al. \(2017\)](#). The encoder consists of three convolutional layers followed by a vector quantiser, and the decoder similarly consists of three convolutional layers.

Training is done on a training dataset over 50 epochs with a batch size of 256. First, we train the VQ-VAEs on typical sources drawn from the labelled data, under the assumption that the model that was not exposed to exotic sources will be better at reconstructing typical sources compared to exotic sources. A score is subsequently assigned to each image in the test set based on the reconstruction error. We expect a trained VQ-VAE model to produce lower reconstruction errors for typical sources. Thus, we associate poorer reconstruction with more anomalous sources, and use a threshold to select exotic sources.

As a separate experiment, we also train the VQ-VAEs on mixed, unlabelled sources, expected to contain both typical and exotic sources. This allows us to use a much larger total number of sources for training with the aim of improving model performance. As the fraction of exotic sources found in the data through manual inspection is very low (about 2.8 per cent), we expect the normal sources to dominate the learned data distribution. As such, we expect exotic sources to yield higher reconstruction errors due to their natural scarcity, despite training the VQ-VAE on mixed data. The manually labelled data is not used during training, but is used at test time to verify the ability of the fully unsupervised VQ-VAE to discriminate between typical and anomalous sources.

To compare the semi-supervised approach (training on typical sources only) to the unsupervised approach (training on all unlabelled data), we consider three configurations as per Table 2. In configuration A, we train the model with typical sources only, while B and C use unlabelled, mixed data to train in a fully unsupervised manner. We can more directly compare the results from A and B, as both use testing sets in which the number of typical and exotic sources are equal, while C provides a more realistic use case, in which the typical sources far outweigh the exotic sources.

² <https://zenodo.org/records/18161425>

³ https://github.com/keras-team/keras-io/blob/master/examples/generative/vq_vae.py

⁴ Chollet, François and others, <https://keras.io>

Sourcename	RA (J2000)	Dec (J2000)	Classification
J1238-4813	12h38m31.2s	-48d13m15.6s	TYPICAL
J2250-1632	22h50m13.68s	-16d32m20.4s	TYPICAL
J1535-4632	22h50m13.68s	-46d32m24s	TYPICAL
J1419-5417	14h19m19.2s	-54d17m13.2s	EXOTIC
J0005-2429	00h05m47.52s	-24d29m31.2s	EXOTIC

Table 1. An excerpt from the full table of labelled data used in this study, with the first column giving the source name, second and third columns giving the centre of the cutout image in Right Ascension and Declination (J2000 epoch) and the classification between “Exotic” and “Typical” sources given in the final column. The full table of 2107 sources is provided on Zenodo in form of a “live” repository, with separate data releases marking adding more sources and tag specificity.

Configuration	Training Set	Exotic Images	Testing Images
A	1991 labelled typical images	58	58
B	13824 unlabelled images	58	58
C	13824 unlabelled images	58	2049

Table 2. The three configurations in which the VQ-VAEs were trained and tested, listing the training data as well as the number of each type of source used in the testing sets.

3.2 Performance Evaluation

Sources correctly identified as exotic are referred to as true positives (TP). Similarly, those correctly identified as typical sources are referred to as true negatives (TN), and those incorrectly identified as exotic or typical false positives (FP) and false negatives (FN), respectively.

The models are trained and tested 35 times each to provide a better statistical understanding of their performance. For configurations A and B, we test the models with equal numbers of typical and exotic sources. As the number of exotic sources is very limited, even in a survey as large as MGCLS, we use the entire set of 58 labelled exotic sources each time. The labelled typical sources are split into sets of equal size, each set having 58 sources to match the number of exotic sources, resulting in 35 sets. The model is retrained and retested for each of these sets. For configuration A, the remainder of the labelled typical sources are used to train the model for each of the 35 sets.

In order to evaluate how well the VQ-VAE has reconstructed a particular image, the input and output images are compared by calculating the normalised cross-correlation (NCC). NCC is a widely used similarity measure that is similar to convolution, and is somewhat invariant to changes in brightness and contrast. For two 2-dimensional arrays, I and K , of m by n pixels, it is given by

$$(I * K)(i, j) = \sum_m \sum_n I(i + m, j + n)K(m, n). \quad (1)$$

NCC is used in order to account for variations in intensity and background noise that should ideally not affect the outcome of the similarity measurement. The NCC measure for two images f and t with dimensions $m \times n$ is

$$NCC = \frac{1}{mn} \sum_x \sum_y \frac{1}{\sigma_f \sigma_t} (f(x, y) - \mu_f)(t(x, y) - \mu_t), \quad (2)$$

where σ and μ are the standard deviation and mean of each image, respectively. The value is averaged over all pixels, and is equal to 1 only if the images are identical. We use the NCC between the original and reconstructed images as our similarity score, with more exotic sources being expected to have a lower NCC score.

We can use the testing set to create a receiver operating characteristic (ROC) curve for a particular model. ROCs are a widely used metric in binary classification, and constitute a plot between the false positive rate (FPR) and true positive rate (TPR) at varied binary classification threshold values. This is the threshold value at which a reconstruction score indicates a source to be exotic rather than typical. TPR, also called recall, is the fraction of positive results that are true TPs. FPR is the fraction of negative samples that are reported as FPs. In case of perfect classification, FPR should be 0, while TPR should be 1. The area under this curve (AUC) is a common metric of success for binary classifiers.

Another common performance metric for a binary classifier is the harmonic mean of the precision and recall, or F-Score. The F_1 score represents the harmonic mean of these two quantities in which they are weighted equally, although a more general form, F_β , applies different weights to the two metrics. In our particular application, it may be more beneficial to favour recall over precision, and contend with more false positives in order to locate more scientifically interesting unusual sources. Therefore, we test both the more common F_1 score, as well as the F_2 score, in which recall is given twice the weight of precision.

In order to determine the appropriate anomaly classification thresholds, we split the testing into two smaller equal sets. The first is used to determine the best thresholds for F_1 and F_2 . The second is used to determine the F_1 and F_2 scores given those thresholds and construct a confusion matrix.

To better assess the ability of VQ-VAE to separate the anomalous from normal sources in its internal (latent) representation, we analyse the resulting latent spaces using t-distributed stochastic nearest neighbour embedding (t-SNE, van der Maaten & Hinton 2008) and uniform manifold approximation and projection⁵ (UMAP, McInnes et al. 2018). Both of these techniques are designed to visualise high-dimensional data by projecting it down into a 2 or 3-dimensional representation. By projecting the encoded latent space representations of the testing images onto a 2D plane, we may examine the separation of the encoded forms of the typical and exotic sources.

4 RESULTS

4.1 Configuration A: Training on Labelled Data

The test set for configuration A is composed of an equal number of exotic and typical sources drawn from the labelled data. The remaining typical sources from the labelled data form the training set. As such, VQ-VAE is trained on typical sources only.

For this configuration with equally large typical and exotic testing sets, the expected F_1 and F_2 scores of a random guess would be 0.5. The AUC of a random guess would also be 0.5.

Figure 2 shows the distribution of the actual F_1 and F_2 scores from testing. The mean F_1 score was 0.7762 with a standard deviation of

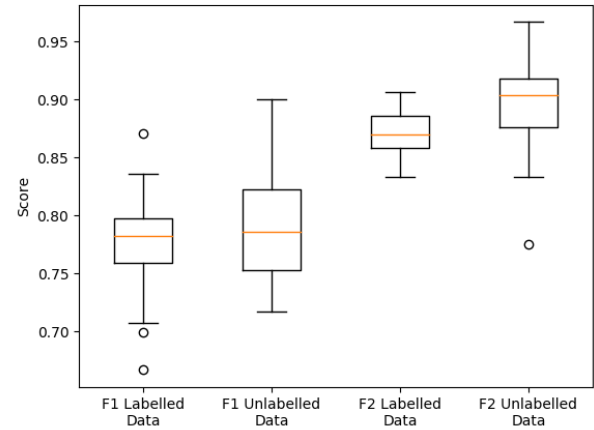


Figure 2. Comparison of the distribution of F_1 and F_2 scores for models in configurations A and B. Models in configuration A are trained on labelled data while those in configuration B are trained on the unlabelled data. Both are tested with testing sets having an equal number of exotic and typical sources. The five number summary for each distribution shows the median in the centre of the box, with half of all values falling within the box. The whiskers show the minimum and maximum, excluding the outliers which are marked by circles.

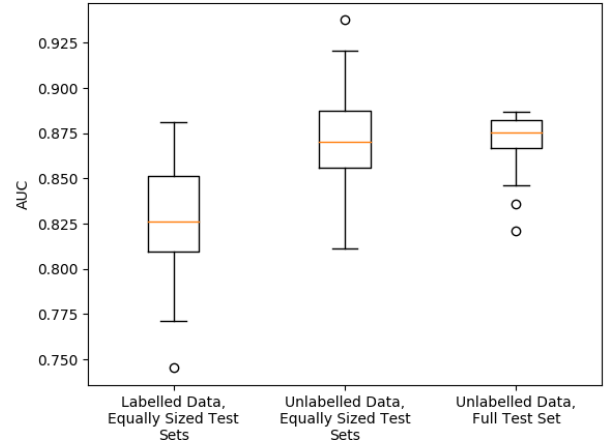


Figure 3. (Left) Box and whisker diagram for AUC in configuration A (Centre) Box and whisker diagram for AUC in configuration B (Right) Box and whisker diagram for AUC in configuration C. The five number summary for each distribution shows the median in the centre of the box, with half of all values falling within the box. The whiskers show the minimum and maximum, excluding the outliers which are marked by circles.

0.0407 and a median of 0.7826. The mean F_2 score was 0.8720 with a standard deviation of 0.0178 and a median of 0.8696. The model is trained and evaluated 35 times, once for each of the 35 training sets, and the results are computed over all 35 runs. As shown in Figure 3, the mean AUC for the ROC was 0.8270 with a standard deviation of 0.0298. These numbers are significantly higher than the expected scores of randomly guessing. As such, we conclude that the model manages to discriminate between the types of sources. The average confusion matrices are shown in Figure 4.

⁵ <https://github.com/lmcinnes/umap>

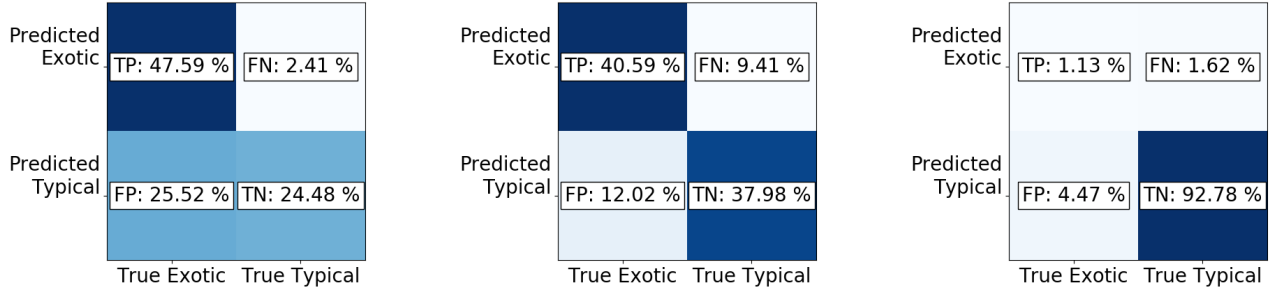


Figure 4. Averaged confusion matrix of the model in configuration A, trained on labelled typical images with an equal number of typical and exotic images in the test set (left). Averaged confusion matrix of the model in configuration B, trained on all unlabelled images with an equal number of typical and exotic images in the test set (centre). Averaged confusion matrix of the model in configuration C trained on all unlabelled images with all labelled images being used for the test set (right).

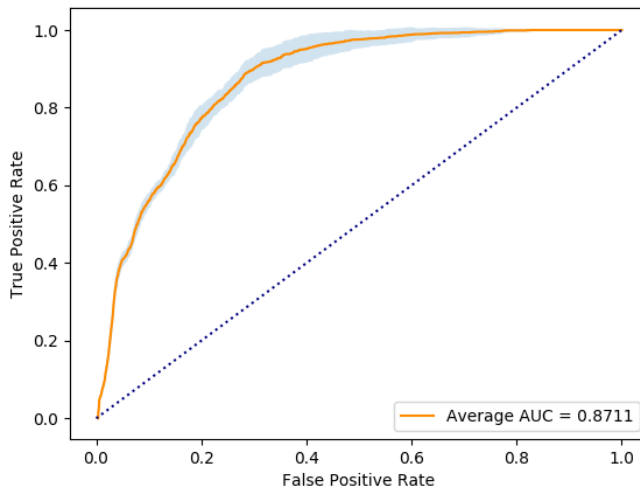


Figure 5. Average ROC with AUC of the VQ-VAE in configuration B with labelled training data and tested on equally sized test sets. The shaded region represents the standard deviation in the curve.

Figure 5 shows the average ROC with deviation of these tests. We can see that the ROC sits well above the line that a random class selection would follow, as suggested by the AUC. In line with the F-scores and the AUC, the ROC suggests that the model is indeed able to distinguish between the sources.

We further analyse the efficacy of VQ-VAE by selecting one of the runs, and inspecting its latent space using t-SNE and UMAP 2D projections. Figures 6 shows the t-SNE and UMAP mappings of the code forms of the test set. Both t-SNE and UMAP show two distinct clusters, corresponding to the typical and anomalous sources. While there is some overlap between the clusters, it is clear that some degree of separation has been obtained. UMAP in particular shows very clear cluster separation. It is evident from Figure 6 that VQ-VAE is more likely to misclassify a typical source as an exotic (FP) than an exotic as a typical (FN), which is a desirable property.

As such, although VQ-VAE shows initial promise, the performance of the model is not sufficient to be deployed in a fully autonomous fashion without manual inspection. Indeed, that is the intention: that expert astronomers take over to assess ambiguous cases in a small fraction of the total number of sources.

4.2 Configuration B: Training on Unlabelled Data

In this configuration, we train the model on all of the unlabelled data. The model is then tested on an equal number of typical and exotic sources from the labelled data. All of the exotic data are used to test the model during each run. An equal number of typical sources are drawn from the labelled data for testing. The model is trained and tested 35 independent times, using a different set of the labelled testing data each run. These results are averaged together.

Figure 2 shows how the F_1 and F_2 scores differ from those of the models trained on labelled data. The mean F_1 score is 0.7900 with a median of 0.7857 and a standard deviation of 0.0462. The mean F_2 score is 0.8970 with a median of 0.9032 and a standard deviation of 0.0363. We see that the performance has improved slightly compared to configuration A. This is likely due to using a significantly larger training set. Figure 3 provides a comparison of the AUC for the different configurations, once again confirming a noticeable improvement in performance. The mean AUC for configuration B is 0.8711 with a median of 0.8701 and a standard deviation of 0.0291. Although the training data contains approximately 2.8% exotic sources (based on the ratio observed in the labelled set), a significantly increased total number of sources to train on leads to a significant improvement in source reconstruction. Since the vast majority of sources are typical, reconstruction of the atypical sources remains a harder task. Figure 7 shows the average ROC for configuration B. As expected from the AUC, we see that the ROC indicates good performance well above random, with slightly better AUC than that of configuration A. Figure 8 show the testing data projected onto the latent space for one run of the configuration using UMAP and t-SNE. Similarly to configuration A, we can see some clustering of the typical and exotic sources by type.

We also perform the Mann–Whitney U (Mann & Whitney 1947) test on the ROC values to compare the increase in performance from training on the larger data set of unlabelled sources over that of training on the smaller set of labelled sources. The null hypothesis is that the medians of the sets of F_1 scores produced by these two methods are the same. The p-value of the test is 0.00034, indicating that the result is significant at $p < 0.05$. As such, there is a statistically significant improvement in performance when training on a larger set of unlabelled data.

The model in configuration B significantly improves upon the performance of configuration A. While the results may still require a post-hoc manual inspection, the burden of labelling a subset of sources as typical prior to training is alleviated in this setup. Con-

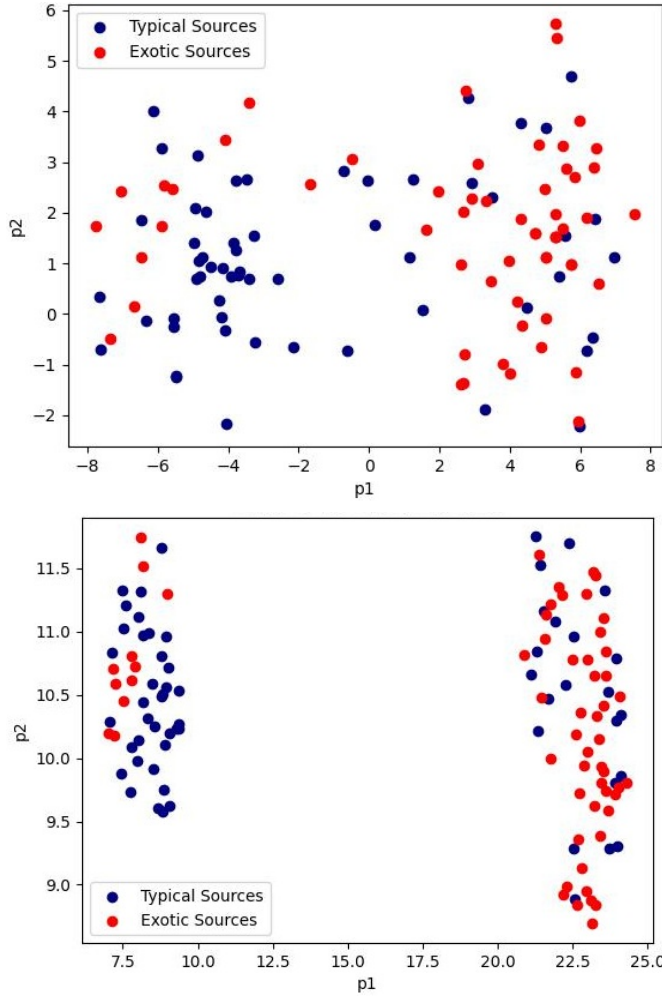


Figure 6. (Top) t-SNE in 2D of the code forms of the testing set from a run of the VQ-VAE in configuration A trained with labelled typical sources. The test set consists of an equal number of typical and exotic sources, with the t-SNE mappings of their code forms shown in blue and red dots respectively. (Bottom) UMAP of the code forms of the testing set from a run of the VQ-VAE trained with labelled typical sources. The test set consists of an equal number of typical and exotic sources, with the UMAP mappings of their code forms show in blue and red dots respectively.

figuration B clearly demonstrates that the larger training set more than makes up for the presence of exotic sources in VQ-VAE training. Training on unlabelled, larger datasets seem to be a promising direction.

4.3 Configuration C: Testing with the full test set

For the final configuration, we train the model on all unlabelled data, and the testing set consists of all labelled data. The model itself is identical to the second configuration, but is tested in a more realistic manner, with a testing set that more closely resembles the distribution of sources found in real data.

We run this configuration 35 times as well to account for stochasticity arising from random model initialisation and data subsampling during training (i.e., mini-batching). All of the data is used in each run, but shuffled so that the same data is not used for finding thresholds and calculating test metrics.

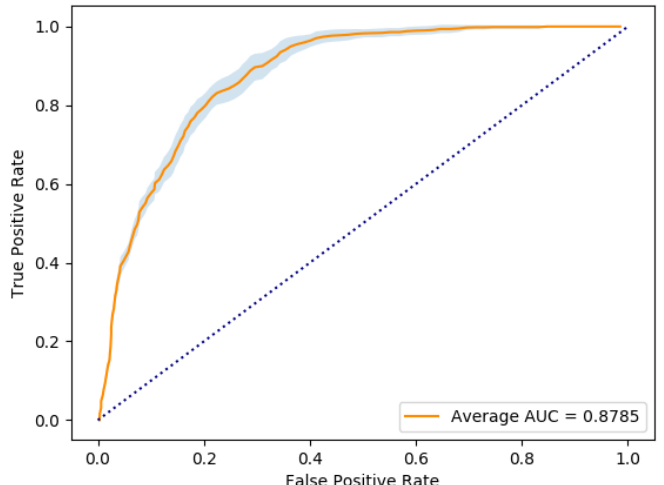


Figure 7. Averaged ROC of the VQ-VAE with unlabelled training data and tested with an equally sized testing set (Configuration B). The shaded region represents the standard deviation of the curve.

The labelled data consists of 2.8% exotic sources, which gives the expected F_1 and F_2 scores of a random guess of 0.052 and 0.028, respectively.

Figure 9 shows the distribution of F_1 and F_2 scores for configuration C. The mean F_1 score is 0.2107 with a median of 0.1880 and a standard deviation of 0.0629, significantly better than random class selection. Likewise, the mean F_2 score is 0.2714 with a median of 0.2900 and a standard deviation of 0.0709. These scores are significantly better than random, but are still low enough to show how difficult it can be to extract such a small fraction of exotic sources. This configuration puts the results from configuration B into context, and demonstrates the complexity of the real-world scenario. The models may be a useful tool, but cannot be used in isolation or without expert intervention.

Figure 3 shows the AUC compared to that of configurations A and B. We see that the performance indicated by the AUC is very similar to that of configurations A and B, although with a smaller deviation. This is most likely due to the difference in testing sets. Similarity between AUCs of configurations B and C is expected, as they are trained on the same data.

The average ROC of these runs is shown in Figure 10, where the mean AUC is 0.8717 with a standard deviation of 0.0118. As expected, it is quite similar to that of configuration B.

The t-SNE and UMAP visualisations for a single run of configuration C are shown in Figure 11. Although some clustering of the exotic and typical sources is evident, the separation is not clear or linear. As in Configuration A, we can see that even a small fraction of the typical sources can create a large overlap with the mappings of the anomalous sources.

4.4 A Sample of Automatically Selected Anomalous Sources

To illustrate the types of sources that may be found in the MGCLS data using VQ-VAE, we select some of the sources from the exotic, typical and unlabelled datasets and show them along with their reconstructions. We manually select five samples from the sources with the highest NCC (a score that indicates that the model reconstructed the source well, thus the source is more typical) and those with the lowest NCC (a score indicating that the model reconstructed

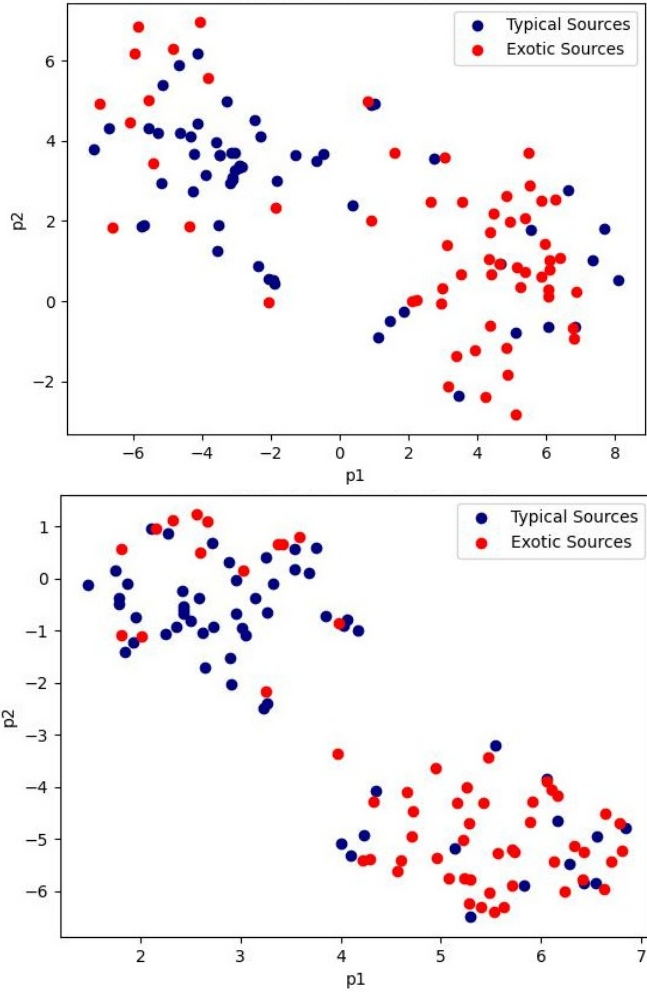


Figure 8. (Top) t-SNE in 2D of the code forms of the testing set from a run of the VQ-VAE in configuration B trained with labelled typical sources. The test set consists of an equal number of typical and exotic sources, with the t-SNE mappings of their code forms shown in blue and red dots respectively. (Bottom) UMAP of the code forms of the testing set from a run of the VQ-VAE trained with labelled typical sources. The test set consists of an equal number of typical and exotic sources, with the UMAP mappings of their code forms show in blue and red dots respectively.

the source poorly, suggesting that the source is anomalous) for each type of source. The NCC scores were determined by a particular run of a model in configuration C.

In Figure 12, which shows sources manually labelled as typical, we can see true negatives with higher NCCs, as well as some false negatives which have low NCCs. Although all sources in Figure 12 were labelled as typical by the astronomers, it is clear that the sources falsely labelled as exotic by VQ-VAE indeed have more nuanced structure. It is important to note that the notion of “exotic” is subjective in itself, and what may be “typical” to an astronomer may still pose a significant challenge to a model learning source reconstruction.

In Figure 13, we show sources manually labelled as anomalous. Here, the sources with the lower NCCs represent true positives, while those with higher NCCs are false negatives, and would be lost amongst the typical sources if classified automatically using VQ-VAE. Notably, the false negatives can all be described as “fuzzy” and

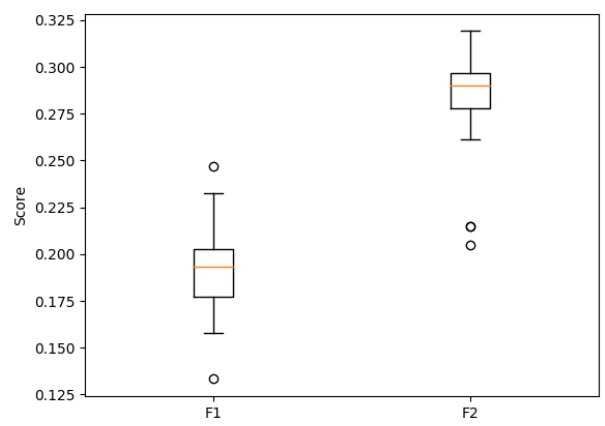


Figure 9. Distribution of F_1 and F_2 scores for models trained on unlabelled data and tested on the full labelled dataset (Configuration C). The five number summary for each distribution shows the median in the centre of the box, half of all values fall within the box. The whiskers show the minimum and maximum, excluding the outliers which are marked by circles.

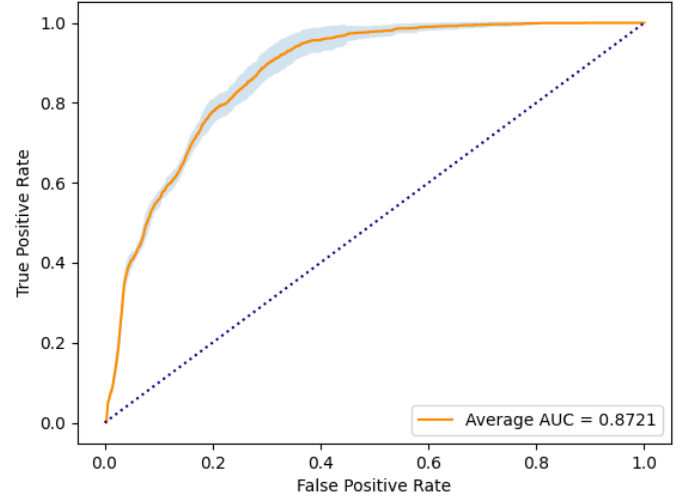


Figure 10. Averaged ROC of the VQ-VAE with unlabelled training data and tested on all labelled data (Configuration C). The shaded region represents the standard deviation of the curve.

blob-like. Supposedly, it is the lack of high-definition intricate structure around the sources that prevented the model from identifying them as exotic.

Finally, in Figure 14 we show a sample of high NCC and low NCC sources from the unlabelled data. Once again, sources that resemble Gaussian blobs are reconstructed well and are labelled typical, while sources with interesting diffuse emissions were labelled as anomalous. This demonstrates the ability of the model to extract interesting sources from the data, as the more unusual sources indeed tend to have lower NCC scores.

The sources shown in Figures 12 to Figure 14 also demonstrate the high quality of the MeerKAT data. The sources are good candidates for further study, including looking at multiwavelength data, which is beyond the scope of this paper. Once the most interesting sources

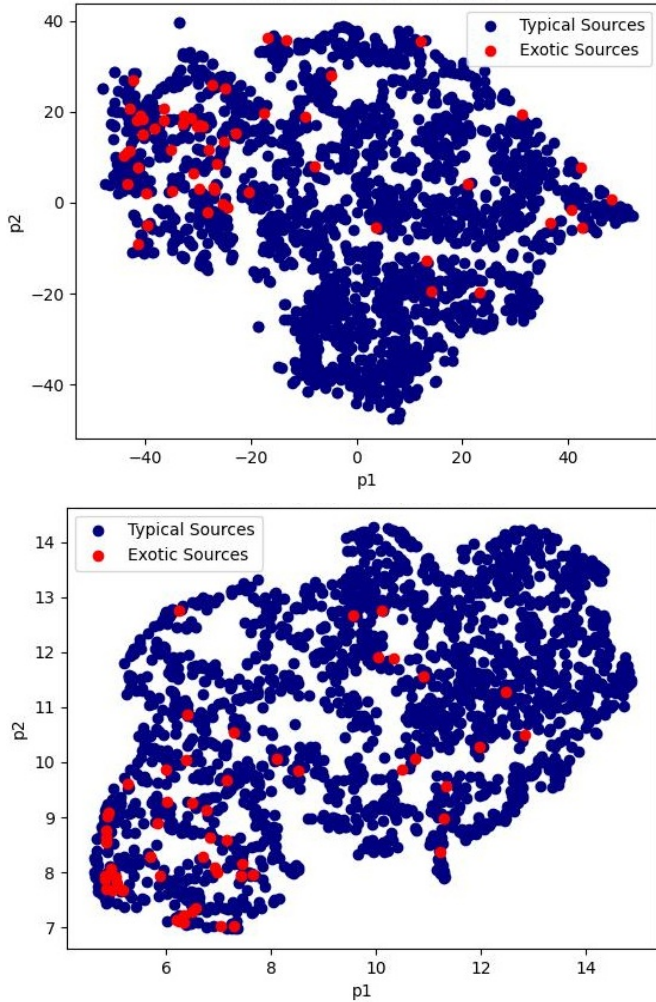


Figure 11. (Top) t-SNE in 2D of the code forms of the testing set from a run of the VQ-VAE in configuration C trained with unlabelled data and tested on the full labelled dataset. The code forms of the typical and exotic labelled data are shown in blue and red, respectively. (Bottom) UMAP of a run of the VQ-VAE in configuration C trained with unlabelled data and tested on the full labelled dataset. The mappings of the code forms of the typical and exotic labelled data are shown in blue and red, respectively.

have been identified, multiwavelength data for them may be obtained, and various properties as well as their environment may be analysed to find possible reasons for their unusual morphologies.

5 CONCLUSION AND OUTLOOK

In this work, we demonstrated the application of vector quantised variational Autoencoders (VQ-VAEs) to 1.28 GHz radio continuum images from the MeerKAT Galaxy Cluster Legacy Survey (MG-CLS). By learning a compact, discrete representation of the data distribution, VQ-VAEs can effectively highlight sources that deviate from typical morphologies, making them well-suited for anomaly detection in large astronomical datasets. Our results showed that VQ-VAEs, even when trained in an unsupervised manner, can filter out the majority of common sources while isolating potentially interesting or unusual structures. We also release a labelled test set of MGCLS radio galaxies to support further research.

The classifications produced by unsupervised VQ-VAE tested in this paper, while not sufficient to be relied upon without further inspection, can significantly reduce the workload of an astronomer faced with tens or hundreds of thousands of sources. For well-selected anomaly thresholds, VQ-VAE returned the most exotic sources and excluded the most typical sources. A fairly high number of false positives resulted from certain sources labelled by astronomers as exotic having blob-like shapes and the lack of finely structured detail. The low number of exotic sources in the data implies that the true positives may still be outnumbered by false positives. The use case and value in VQ-VAE is to help the user automatically search through large collections of potential sources by reducing the total number without discarding the majority of exotic sources. By carefully configuring the anomaly threshold, VQ-VAE may be able to remove a large proportion of the typical sources while retaining almost all of the exotic sources.

Many sources may be classified as exotic by experts because of a deeper understanding of the source itself, while not having features that are particularly unusual in shape. For automated classification, a method that considers other properties of a source, such as multiwavelength data, may likewise outperform a model that classifies purely in the radio image plane. It should also be noted that the categories used of “typical” and “exotic” are very broad and inherently subjective. Searching for a more narrowly defined type of morphology, such as X-shaped sources or bent tail sources, may yield stronger results. VQ-VAEs are a promising candidate for further development in this area. We intend to explore these options, as well as apply VQ-VAEs to other large radio surveys, such as the recent MeerKAT survey on the South Pole Telescope (SPT) survey field.

Automated approaches such as the one proposed in this paper remain key to searching through high volumes of data and extracting the full scientific potential of new and upcoming telescopes such as the SKA and its pathfinders that have massively increased depth, area, imaging fidelity, and dynamic range. In addition, the set of 2107 labelled MeerKAT source images, which we make freely available, forms a resource of considerable value for the community, which we aim to maintain in a “live” form with frequent updates for additional sources and classification tags.

6 ACKNOWLEDGEMENTS

F.L. Ventura acknowledges financial support from the Inter-University Institute for Data Intensive Astronomy (IDIA). IDIA is a partnership of the University of Cape Town, the University of Pretoria and the University of the Western Cape. IDIA is registered on the Research Organization Registry with ROR ID 01edhw26, and on Open Funder Registry with funder ID 100031500. RPD acknowledges funding from the South African Radio Astronomy Observatory (SARAO), which is a facility of the National Research Foundation (NRF), an agency of the Department of Science, Technology and Innovation (DSTI). RPD also acknowledges funding from the South African Research Chairs Initiative of the DSTI/NRF (Grant ID: 77948). We acknowledge the use of the ilifu cloud computing facility – www.ilifu.ac.za, a partnership between the University of Cape Town, the University of the Western Cape, Stellenbosch University, Sol Plaatje University and the Cape Peninsula University of Technology. The ilifu facility is supported by contributions from the Inter-University Institute for Data Intensive Astronomy (IDIA – a partnership between the University of Cape Town, the University of Pretoria and the University of the Western Cape), the Computational Biology division at UCT and the Data Intensive Research Initiative

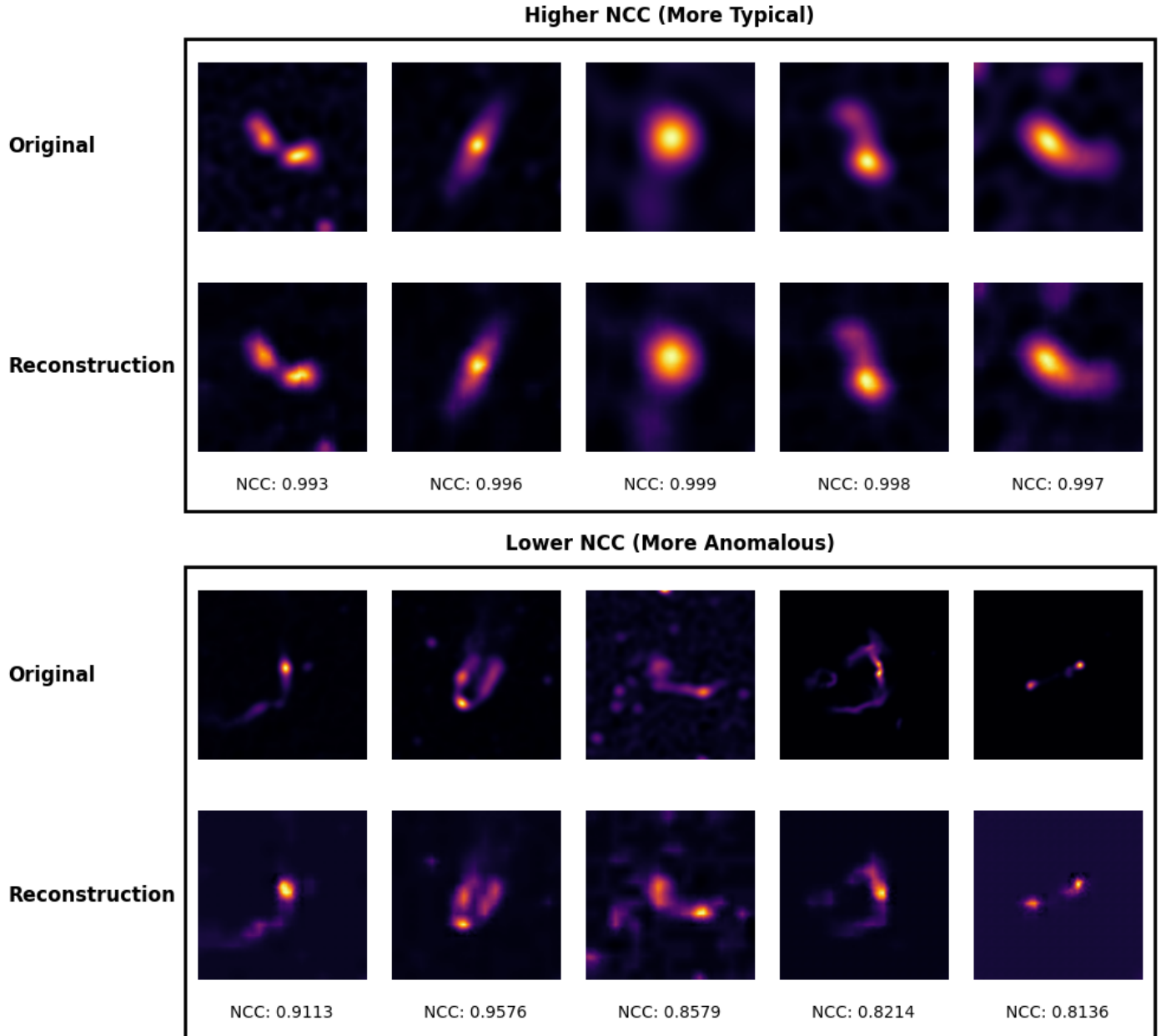


Figure 12. A sample of the best and worst reconstructed typical sources with their reconstructions as performed by a VQ-VAE trained on the unlabelled data. (Top) Five of the best reconstructed typical sources, having the highest scores and therefore ranked as "most typical." They are shown with their reconstructions as well as the reconstruction score. (Below) Five of the worst reconstructed typical sources, having the lowest scores and therefore ranked as "least typical". These sources come up as false positives. They are shown with their reconstructions and reconstruction scores.

of South Africa (DIRISA). The MeerKAT telescope is operated by the South African Radio Astronomy Observatory, which is a facility of the National Research Foundation, an agency of the Department of Science, Technology and Innovation.

7 DATA AVAILABILITY

The data underlying this article are available in Zenodo, at <https://zenodo.org/records/18161425>. The datasets were derived from the MeerKAT Galaxy Cluster Legacy Survey (Knowles et al. 2022) available at <https://doi.org/10.48479/7epd-w356>.

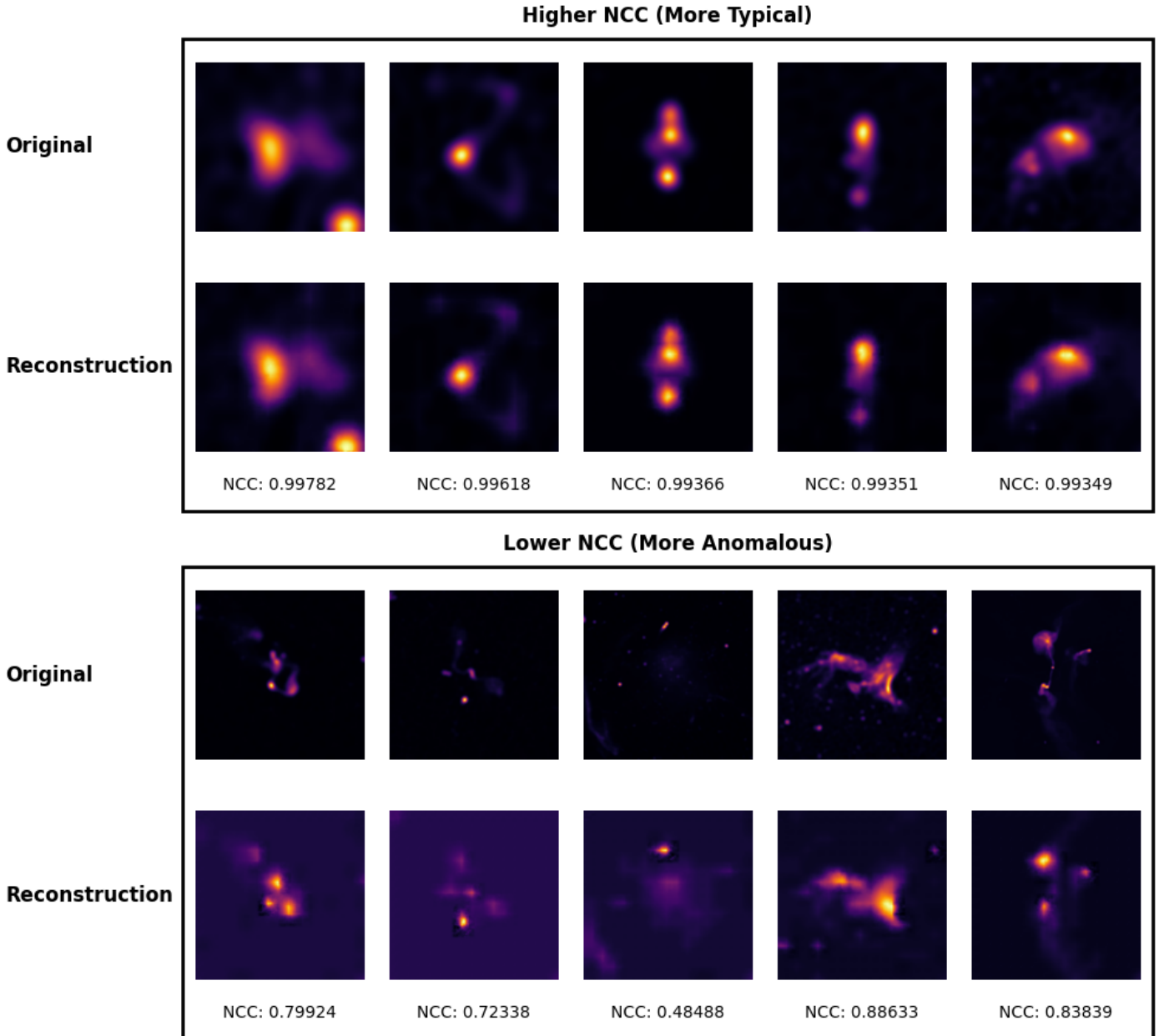


Figure 13. A sample of the best and worst reconstructed exotic sources with their reconstructions as performed by a VQ-VAE trained on the unlabelled data. (Top) Five of the best reconstructed exotic sources, having the highest scores and therefore ranked as "most typical." These sources are false negatives. They are shown with their reconstructions as well as the reconstruction score. (Below) Five of the worst reconstructed exotic sources, having the lowest scores and therefore ranked as "least typical". They are shown with their reconstructions and reconstruction scores.

REFERENCES

Alonso P., Zhang J., Li X.-D., 2024, AJ, 167, 129
 Andrianomena S., Tang H., 2024, J. Cosmology Astropart. Phys., 2024, 034
 Becker R. H., White R. L., Helfand D. J., 1995, *ApJ*, 450, 559
 Brand K., Grobler T. L., Kleynhans W., 2025, RAS Techniques and Instruments, 4, rza005

Condon J. J., Cotton W. D., Greisen E. W., Yin Q. F., Perley R. A., Taylor G. B., Broderick J. J., 1998, *AJ*, 115, 1693
 Doorenbos L., Cavuoti S., Brescia M., D'Isanto A., Longo G., 2021, Comparison of Outlier Detection Methods on Astronomical Image Data. Springer International Publishing, Cham, pp 197–223, doi:10.1007/978-3-030-65867-0_9, https://doi.org/10.1007/978-3-030-65867-0_9
 Gangloff H., Pham M.-T., Courtrai L., Lefèvre S., 2022, in 2022 26th In-

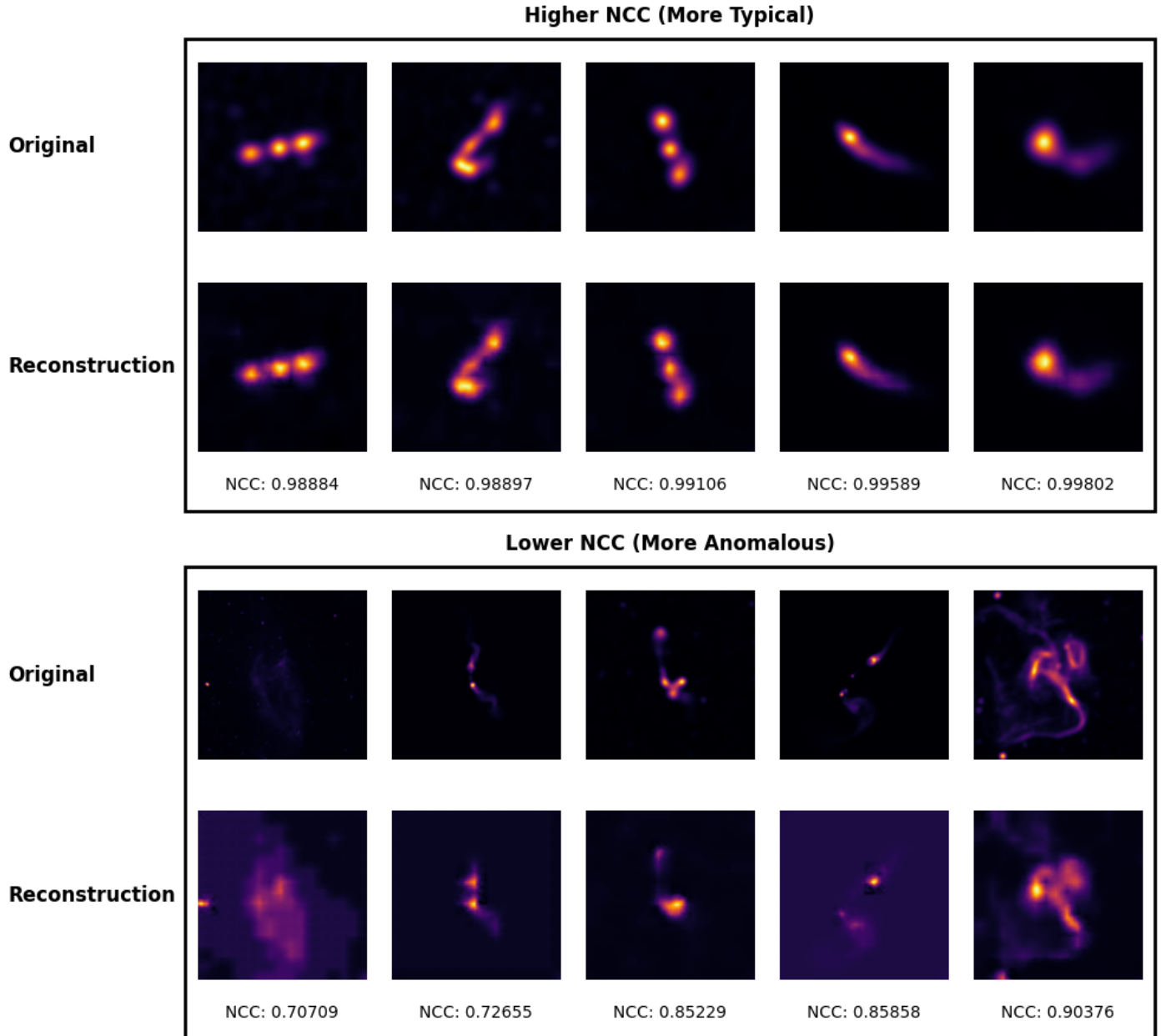


Figure 14. A sample of the best and worst reconstructed sources from the unlabelled data with their reconstructions as performed by a VQ-VAE trained on the unlabelled data. (Top) Five of the best reconstructed sources, having the highest scores and therefore ranked as "most typical." They are shown with their reconstructions as well as the reconstruction score. (Below) Five of the worst reconstructed sources, having the lowest scores and therefore ranked as "least typical". They are shown with their reconstructions and reconstruction scores.

ternational Conference on Pattern Recognition (ICPR). pp 435–441, [doi:10.1109/ICPR56361.2022.9956102](https://doi.org/10.1109/ICPR56361.2022.9956102)
 Giger M., Csillaghy A., 2024, Space Weather, 22, e2023SW003516
 Han Y., Zou Z., Li N., Chen Y., 2022, Research in Astronomy and Astrophysics, 22, 085006
 Jebril H., Esengönül M., Bogunović H., 2024, Bioengineering, 11, 682
 Knowles K., et al., 2022, [A&A](#), 657, A56
 Lochner M., Bassett B., 2021, [Astronomy and Computing](#), 36, 100481

Lochner M., Rudnick L., 2025, [AJ](#), 169, 121
 Mann H. B., Whitney D. R., 1947, [The Annals of Mathematical Statistics](#), 18, 50
 Marimont S. N., Tarroni G., 2021, in 2021 IEEE 18th International Symposium on Biomedical Imaging (ISBI). pp 1764–1767
 McInnes L., Healy J., Saul N., Großberger L., 2018, [Journal of Open Source Software](#), 3, 861
 Pinaya W. H., Tudosi P.-D., Gray R., Rees G., Nachev P., Ourselin S., Cardoso

M. J., 2022, Medical Image Analysis, 79, 102475

Van Den Oord A., Vinyals O., et al., 2017, Advances in neural information processing systems, 30

van den Oord A., Vinyals O., kavukcuoglu k., 2017, in Guyon I., Luxburg U. V., Bengio S., Wallach H., Fergus R., Vishwanathan S., Garnett R., eds, Vol. 30, Advances in Neural Information Processing Systems. Curran Associates, Inc., https://proceedings.neurips.cc/paper_files/paper/2017/file/7a98af17e63a0ac09ce2e96d03992fbc-Paper.pdf

van der Maaten L., Hinton G., 2008, Journal of Machine Learning Research, 9, 2579

This paper has been typeset from a \TeX / \LaTeX file prepared by the author.